Korean J. Chem. Eng., **27**(4), 1132-1138 (2010)
DOI: 10.1007/s11814-010-0212-9

Steam reforming of liquid petroleum gas over Mn-promoted Ni/γ-Al_2O_3 catalysts

Jae Hyun Park*, Doohwan Lee, Hyun Chul Lee**, and Eun Duck Park*,†**

*Division of Energy Systems Research and Division of Chemical Engineering and Materials Engineering, Ajou University, Wonchun-dong Yeongtong-gu, Suwon 443-749, Korea
**Energy and Environment Laboratory, Samsung Advanced Institute of Technology (SAIT), P. O. Box 111, Suwon 440-600, Korea
(*Received 1 February 2010 • accepted 19 March 2010*)

Abstract−Three different Mn-promoted Ni/γ-Al_2O_3 catalysts, Mn/Ni/γ-Al_2O_3, Mn-Ni/γ-Al_2O_3 and Ni/Mn/γ-Al_2O_3, were prepared and applied to the steam reforming of liquid petroleum gas (LPG) mainly composed of propane and butane. For comparison, Ni/γ-Al_2O_3 catalysts containing different amount of Ni were also examined. In the case of the Ni/γ-Al_2O_3 catalysts, 4.1 wt% Ni/γ-Al_2O_3 showed the stable catalytic activity with the least amount of coke formation. Among the various Mn-promoted Ni/γ-Al_2O_3 catalysts, Mn/Ni/γ-Al_2O_3 showed the stable catalytic activity with the least amount of coke formation. It also exhibited a similar H_2 formation rate compared with Ni/γ-Al_2O_3. Several characterization techniques--N_2 adsorption/desorption, X-ray diffraction (XRD), CO chemisorptions, temperature-programmed reduction (TPR), X-ray photoelectron spectroscopy (XPS) and CHNS analysis--were employed to characterize the catalysts. The catalytic activity increased with increasing amount of chemisorbed CO for the Mn-promoted Ni/γ-Al_2O_3 catalysts. The highest proportion of Mn^{4+} species was observed for the most stable catalyst.

Key words: Steam Reforming, Nickel, Manganese Oxides, Hydrogen, LPG

INTRODUCTION

Due to the progress made in fuel cells, hydrogen is attracting increasing attention [1]. Currently, it is generally produced from various hydrocarbons through a series of catalytic processes including the reforming and water-gas shift reaction. Among the various hydrocarbons, liquefied petroleum gas (LPG), which is mainly composed of propane and butane, is quite attractive, because it has high potential as a hydrogen carrier for fuel cells [2]. Since LPG can be easily distributed through a well-developed infrastructure [3], it is a favorable feedstock for distributed hydrogen production.

Syngas ($CO+H_2$) can be made through several routes such as partial oxidation [4], steam reforming [5,6] and autothermal reforming [7,8]. Although each method has its merits [9], steam reforming has been extensively examined because it enables the highest hydrogen concentration to be obtained in the product stream, thus making it possible to reduce the size of the subsequent purification units used to obtain high-purity hydrogen for fuel cells.

As the steam-reforming catalysts, supported Ni catalysts have been used for industrial steam reforming processes because of their inherent availability and lower cost in comparison to noble metal catalysts [10]. The steam reforming reaction is highly endothermic and therefore requires high operating temperatures to produce a high hydrogen yield. As a result, the nickel particles in the supported Ni catalysts tend to become agglomerated and lose their active surface area under steam reforming conditions [11]. Furthermore, coke formation can be a serious problem over Ni-based catalysts. Therefore, the development of Ni-based catalysts which can resist the formation of coke as well as sintering is essential [12,13].

Until now, a number of studies have been carried out in an attempt to improve the catalytic activity of Ni-based catalysts for the steam reforming of hydrocarbons. Various kinds of support such as MgO, TiO_2, SiO_2, activated carbon, La_2O_3 [14], ZrO_2 [15], and Al_2O_3 have been examined to suppress the formation of carbon [16,17]. It was also suggested that the amount of carbon deposited could be decreased by using nickel supported on metal oxides with strong Lewis basicity [18]. It was suggested that the presence of mobile TiO_x species helped to remove the large ensembles of Ni atoms which are active for coke formation over Ni/TiO_2 [19]. The formation of a partially reducible NiO-MgO solid solution appeared to stabilize the surface Ni atom and prevent carbon diffusion into the nickel particles [20-23].

Besides the support, various kinds of promoters have been examined to suppress the formation of coke over the supported Ni catalysts. Alkali metals, such as K_2O and CaO, were reported to improve the coking resistance by enhancing the carbon gasification but with a loss of catalytic activity [24,25]. Zhuang [14] et al. investigated the effect of cerium oxide as a promoter for the supported Ni catalysts on the steam reforming of methane and found that it increased the steam reforming activity and also decreased the carbon deposition rate. Su and Guo [26] also reported an improvement in the catalytic activity and resistance to Ni sintering for Ni/Al_2O_3 catalysts doped with rare earth oxides in the steam reforming of methane. Moreover, the oxides of heavy rare earth elements (Gd, Er, Dy) [27] exhibited a more pronounced effect than those of the light ones (La, Pr, Nd, Yb) [28,29]. The addition of manganese oxides has been reported to decrease the formation of coke in the dry reforming of methane over Ni/Al_2O_3 [30].

In this work, we prepared three kinds of Mn-promoted Ni/γ-Al_2O_3 catalysts impregnated in different sequence and applied them to the steam reforming of LPG, which can cause much more coke forma-

†To whom correspondence should be addressed.
E-mail: edpark@ajou.ac.kr

tion than the steam reforming of methane. The catalyst stability for each catalyst was examined and discussed based on their characterizations.

EXPERIMENTAL

1. Catalyst Preparation

Supported Ni catalysts containing different amounts of Ni were prepared by impregnating γ-Al_2O_3 with an aqueous solution of $Ni(NO_3)_2$, followed by drying at 393 K and subsequent calcination in air at 973 K for 2 h. Three different Mn-promoted Ni/γ-Al_2O_3 catalysts were prepared as follows. In the case of Mn/Ni/γ-Al_2O_3, Ni/γ-Al_2O_3 was prepared as described above and then impregnated with an aqueous solution of $Mn(NO_3)_2$, followed by drying at 393 K and subsequent calcination in air at 973 K for 2 h. Ni/Mn/γ-Al_2O_3 was prepared in the same way as Mn/Ni/γ-Al_2O_3 except that the manganese precursor was impregnated first before the impregnation of the Ni precursor. Ni-Mn/γ-Al_2O_3 was prepared by a co-impregnation method: Both $Ni(NO_3)_2$ and $Mn(NO_3)_2$ were impregnated on γ-Al_2O_3, followed by drying at 393 K and subsequent calcinations in air at 973 K for 2 h. The Mn content was intended to be 5 wt%. All of the prepared catalysts were reduced in H_2 at 1,173 K for 1 h before the reaction.

2. Catalyst Characterization

The BET surface areas of the calcined catalysts were measured by N_2 adsorption-desorption at 77 K using an Autosorb-1 (Quantachrome) instrument. Before the measurement, the samples were degassed in a vacuum at 473 K for 2 h.

The pulsed CO chemisorptions were conducted in an AutoChem 2910 unit (Micromeritics) equipped with a thermal conductivity detector (TCD) to measure the CO consumption. Quartz U-tube reactors were generally loaded with 0.20 g of the sample. All of the catalysts were pretreated by reduction in H_2 at 1,173 K for 1 h, then cooled to room temperature. The chemisorptions experiments were carried out at 300 K in an He stream at a flow rate of 30 ml/min through the pulsed-chemisorptions technique, in which 500 ml pulses of CO were utilized.

Temperature-programmed reduction (TPR) was conducted in an AutoChem 2910 unit (Micromeritics) equipped with a TCD to measure the H_2 consumption. A water trap composed of blue silica gel removed the moisture from the TPR effluent stream at 273 K before the TCD. Quartz U-tube reactors were generally loaded with 0.20 g of the sample. All of the samples were calcined in air at 973 K for 2 h before the TPR experiment. The TPR patterns were obtained using 10 vol% H_2/Ar at a flow rate of 30 ml/min in the temperature range from 313 K to 1,173 K at a heating rate of 10 K/min, while the TCD signals were monitored after any residual oxygen in the line was removed by flowing He at 313 K for 1 h.

The XRD patterns were recorded on a Rigaku D/MAC-III using Cu Kα radiation (λ=0.15406 nm), operated at 40 kV and 100 mA (4.0 kW). The crystalline size of Ni and Mn_2O_3 was calculated by applying the Scherrer line broadening equation as follows:

$$L = \frac{0.9\lambda_{K_{\alpha 1}}}{B_{(2\theta)}\cos\theta_{max}}$$

where L denotes the average particle size, 0.9 is the value when $B_{(2\theta)}$ is the full width at half maximum (FWHM) of the peak broadening in radians, $\lambda_{K\alpha 1}$ is the wavelength of the X-ray radiation (0.15406 nm), and λ_{max} is the angular position at the (200) peak maximum of Ni.

X-ray photoelectron spectroscopy (XPS) was performed for the reduced catalysts and the catalysts after the reaction with a Micromeritics XPS spectrometer using monochromatic AI-Kα radiation operated at 1,486.6 eV. Reduction was performed with H_2 at 1,173 K for 1 h. The catalysts after the reaction were collected after 10 h of LPG steam reforming.

The amount of carbon formed on the catalysts during the reaction was determined by using a CHNS analyzer (LECO-CHNS-932).

The Ni and Mn contents for each catalyst were analyzed by inductively coupled plasma-atomic emission spectroscopy (ICP-AES, JY-70Plus, Jobin-Yvon).

3. Reactor System and Experimental Procedure

The catalytic activity measurements were carried out in a small fixed bed reactor with the catalysts that had been retained between 45 and 80 mesh sieves. A standard gas consisting of 12.8 mol% C_3H_8, 0.7 mol% n-C_4H_{10} and 82 mol% H_2O balanced with N_2 was fed to the reactor, in which 0.10 g of the catalyst without diluents was loaded. The typical reaction temperature was 873 K. Before the reaction, the catalysts were reduced in situ under H_2 [30 cm^3 (STP)/min)] at 1,173 K for 1 h. The effluent from the reactor was separated with Poraplot-Q and Carbosphere columns and analyzed using a gas chromatograph (HP5890) equipped with the flame ionization detector (FID) and TCD. The formation rate of H_2, r_{H_2}, was calculated by multiplying the exit concentration of H_2 and the effluent flow rate per mass of catalyst.

RESULTS AND DISCUSSION

Ni/γ-Al_2O_3 catalysts containing different amounts of Ni were examined for the steam reforming of LPG to determine the effect of their Ni content on their catalytic activity and stability, as shown in Fig. 1. Under the given reaction conditions, all of the catalysts showed 100% conversions of propane and butane initially. However, reactor plug-

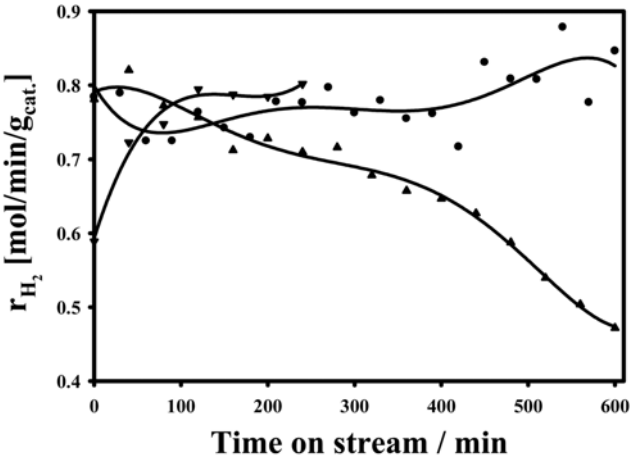

Fig. 1. Comparison of the activity of the γ-Al_2O_3-supported Ni catalysts containing different amounts of Ni, viz. 3.1 wt% Ni (▲), 4.1 wt% Ni (●), and 8.1 wt% Ni (▼). The feed composition was 12.8 mol% C_3H_8, 0.7 mol% n-C_4H_{10} and 82 mol% H_2O in N_2, F/W=533 ml (STP)/min/$g_{cat.}$.

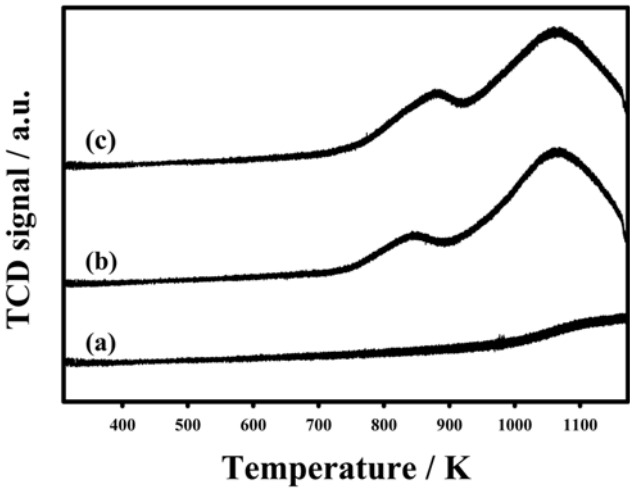

Fig. 2. Temperature-programmed reduction (TPR) patterns for the γ-Al_2O_3-supported Ni catalysts containing different amounts of Ni, viz. 3.1 wt% Ni (a), 4.1 wt% Ni (b), and 8.1 wt% Ni (c).

ging occurred due to the formation of large amounts of coke in the case of the 8.1 wt% Ni/γ-Al_2O_3 catalyst. A gradual decrease in the catalytic activity was observed over 3.1 wt% Ni/γ-Al_2O_3. On the other hand, stable catalytic activity was obtained over 4.1 wt% Ni/γ-Al_2O_3.

To determine the reducibility of the Ni species over the Ni/γ-Al_2O_3 catalysts, temperature-programmed reduction (TPR) patterns were obtained for each sample, as shown in Fig. 2. In the case of the 3.1 wt% Ni/γ-Al_2O_3 catalyst only one TPR peak was observed at around 1,150 K, which may be due to the reduction of $NiAl_2O_4$ [31]. On the other hand, two TPR peaks were observed over both 4.1 wt% Ni/γ-Al_2O_3 and 8.1 wt% Ni/γ-Al_2O_3 at 845-880 K and 1,060 K. The TPR peak at 845-880 K was attributed to the reduction of NiO strongly bound to γ-Al_2O_3 [32]. These results imply that the impregnated Ni species reside on the defect sites of the alumina surface and form $NiAl_2O_4$ after the calcinations step. The formation of separate NiO can occur only after most of the defect sites of the alumina surface are saturated with the Ni species.

XRD patterns were also obtained for each sample before and after the reaction, as shown in Fig. 3. For all of the catalysts, XRD peaks representing Ni were found. The intensity of the XRD peaks representing Ni increased with increasing Ni content. The crystalline size of Ni for 8.1 wt% Ni/γ-Al_2O_3 was calculated by Scherrer's equation and determined to be 13 nm. As shown in Fig. 3(B), the formation of carbon was confirmed after the reaction over 8.1 wt% Ni/γ-Al_2O_3. Therefore, the surface coverage of the metallic Ni with carbon may be one of reasons for the catalyst deactivation.

To determine the cause of the deactivation of the catalyst, the amount of deposited carbon was determined by a CHNS analyzer. The amount of carbon was determined to be 9.6, 7.8 and 63.6 $g_c/g_{cat.}$ for 3.1 wt% Ni/γ-Al_2O_3, 4.1 wt% Ni/γ-Al_2O_3 and 8.1 wt% Ni/γ-Al_2O_3, respectively. Based on this result, it can be said that the deactivation of the catalyst must be due to coke formation. The larger amount of formed carbon over 8.1 wt% Ni/γ-Al_2O_3 than over 4.1 wt% Ni/γ-Al_2O_3 can be explained by the difference in the crystalline size of Ni. As can be seen in Fig. 3, the larger crystalline size

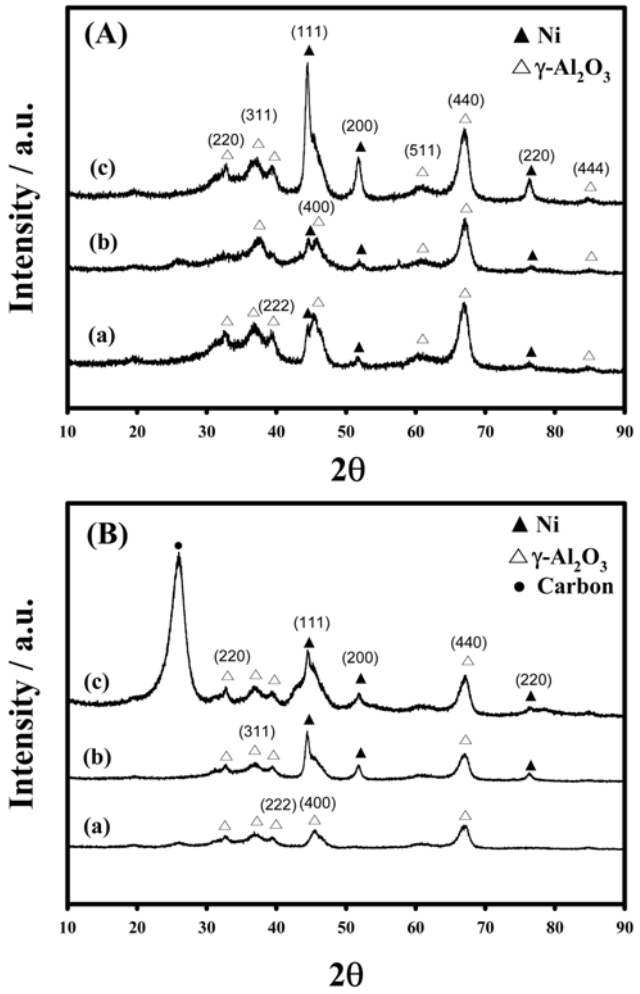

Fig. 3. X-ray diffraction patterns of the γ-Al_2O_3-supported Ni catalysts containing different amounts of Ni, viz. 3.1 wt% Ni (a), 4.1 wt% Ni (b), and 8.1 wt% Ni (c) before (A) and after the reaction (B).

of Ni was observed over 8.1 wt% Ni/γ-Al_2O_3 than over 4.1 wt% Ni/γ-Al_2O_3. It was reported that the formation of filamentous carbon was significantly influenced by the metal particle size and proceeded mostly over the metal particles larger than 7 nm [33]. Therefore, 4.1 wt% Ni/γ-Al_2O_3 was selected as the model catalyst for the subsequent studies.

Three different Mn-promoted γ-Al_2O_3-supported Ni catalysts were prepared and tested for the steam reforming of LPG, as shown in Fig. 4. The catalytic activity decreased in the following order: 5.3 wt% Mn/5.4 wt% Ni/γ-Al_2O_3>4.2 wt% Mn-4.2 wt% Ni/γ-Al_2O_3>> 4.0 wt% Ni/4.5 wt% Mn/γ-Al_2O_3. In the case of the 4.0 wt% Ni/4.5 wt% Mn/γ-Al_2O_3 catalyst, a gradual decrease in the catalytic activity was observed during 10 h of the reaction. The amount of CO chemisorbed at 300 K was determined to be 9.6, 3.4, and 2.6 mmol $CO/g_{cat.}$ for 5.3 wt% Mn/5.4 wt% Ni/γ-Al_2O_3, 4.2 wt% Mn-4.2 wt% Ni/γ-Al_2O_3, 4.0 wt% Ni/4.5 wt% Mn/γ-Al_2O_3, respectively. This is in line with the catalytic activity.

To determine the reducibility of the Ni and Mn species in the Mn-promoted γ-Al_2O_3-supported Ni catalysts, TPR patterns were obtained for each sample, as shown in Fig. 5. For comparison, the TPR pat-

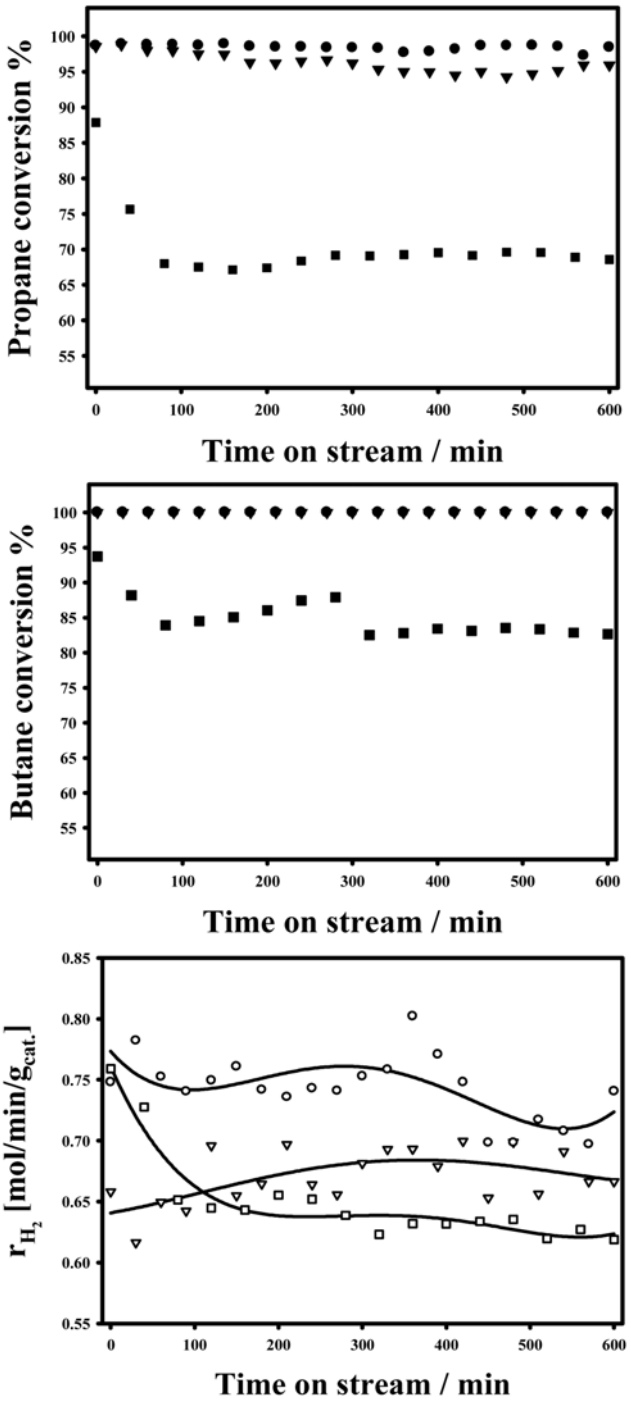

Fig. 4. The catalytic activity for LPG steam reforming over the Mn-promoted Ni/γ-Al_2O_3 catalysts, viz. 5.3 wt% Mn/5.4 wt% Ni/γ-Al_2O_3 (●), 4.0 wt% Ni/4.5 wt% Mn/γ-Al_2O_3 (■), and 4.2 wt% Mn-4.2 wt% Ni/γ-Al_2O_3 (▼). The feed composition was 12.8 mol% C_3H_8, 0.7 mol% n-C_4H_{10} and 82 mol% H_2O in N_2, F/W=533 ml (STP)/min/$g_{cat.}$.

tern for 5 wt% Mn/γ-Al_2O_3 is also presented. For the Mn-promoted γ-Al_2O_3-supported Ni catalysts, a rather broad TPR peak with a maximum at 1,050 K was observed with a shoulder at 850 K. No TPR peak was observed due to the reduction of mixed oxides composed of Mn and Al. As shown in Fig. 2, 4.1 wt% Ni/γ-Al_2O_3 shows two

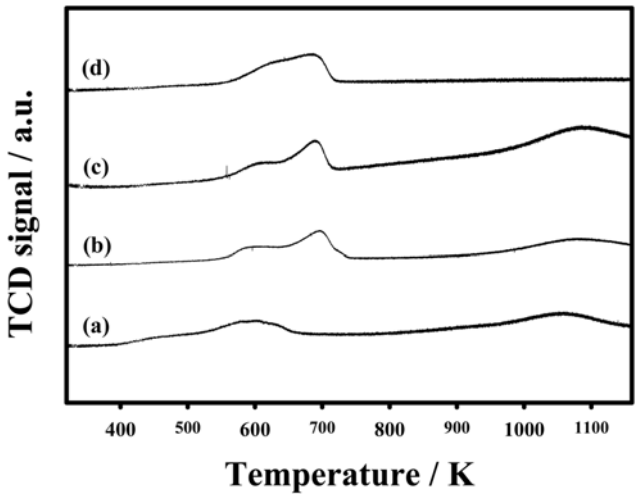

Fig. 5. Temperature-programmed reduction (TPR) patterns for the Mn-promoted Ni/γ-Al_2O_3 catalysts, viz. 5.3 wt% Mn/5.4 wt% Ni/γ-Al_2O_3 (a), 4.0 wt% Ni/4.5 wt% Mn/γ-Al_2O_3 (b), and 4.2 wt% Mn-4.2 wt% Ni/γ-Al_2O_3 (c). The TPR pattern for 5 wt% Mn/γ-Al_2O_3 (d) was also added for comparison.

TPR peaks at around 850 K and 1,050 K due to the reduction of NiO and $NiAl_2O_4$, respectively. TPR peaks due to the reduction of $NiAl_2O_4$ were obtained for all of the Mn-promoted γ-Al_2O_3-supported Ni catalysts, although their intensities differed from each other. The weakest TPR peak at around 1,000 K was observed for 4.0 wt% Ni/4.5 wt% Mn/γ-Al_2O_3, which can be interpreted as meaning that some of the defect sites on the alumina surface are blocked with the Mn species during the calcinations step of Mn/γ-Al_2O_3. The TPR peaks in the range from 550 K to 700 K can be attributed to the reduction of MnO_x species based on the TPR pattern of the 5 wt% Mn/γ-Al_2O_3 catalyst. The only difference in the TPR patterns obtained over the 4.0 wt% Ni/4.5 wt% Mn/γ-Al_2O_3 and 4.2 wt% Mn-4.2 wt% Ni/γ-Al_2O_3 catalysts is the TPR peak intensity. 4.2 wt% Mn-4.2 wt% Ni/γ-Al_2O_3 shows a stronger TPR peak intensity at around 1,000 K than 4.0 wt% Ni/4.5 wt% Mn/γ-Al_2O_3, which is reasonable because $NiAl_2O_4$ can easily be formed over the former catalyst. In the case of 5.3 wt% Mn/5.4 wt% Ni/γ-Al_2O_3, similar TPR peaks were obtained to those observed for the other Mn-promoted Ni/γ-Al_2O_3 catalysts but the TPR peaks at low temperatures were shifted to lower temperatures. This implies that a weak interaction can be formed between the MnO_x species and alumina surface, because some of the defect sites may be blocked by the formation of $NiAl_2O_4$ in 5.3 wt% Mn/5.4 wt% Ni/γ-Al_2O_3.

XRD patterns were obtained to determine the crystalline phase for the Mn-promoted Ni/γ-Al_2O_3 catalysts before and after the reaction, as shown in Fig. 6. The presence of Mn_2O_3 was confirmed for all of the catalysts. The formation of crystalline carbon was also observed after the reaction for all of the catalysts. The amount of carbon formed during the reaction was determined to be 4.0, 24.0, and 8.3 $g_c/g_{cat.}$ for the 5.3 wt% Mn/5.4 wt% Ni/γ-Al_2O_3, 4.2 wt% Mn-4.2 wt% Ni/γ-Al_2O_3, and 4.0 wt% Ni/4.5 wt% Mn/γ-Al_2O_3 catalysts, respectively. It is worth noting that the most active catalyst, 5.3 wt% Mn/5.4 wt% Ni/γ-Al_2O_3, showed the least amount of coke formation. Furthermore, it showed less carbon formation than the 4.1 wt% Ni/γ-Al_2O_3 catalyst. The role of the MnO_x species might

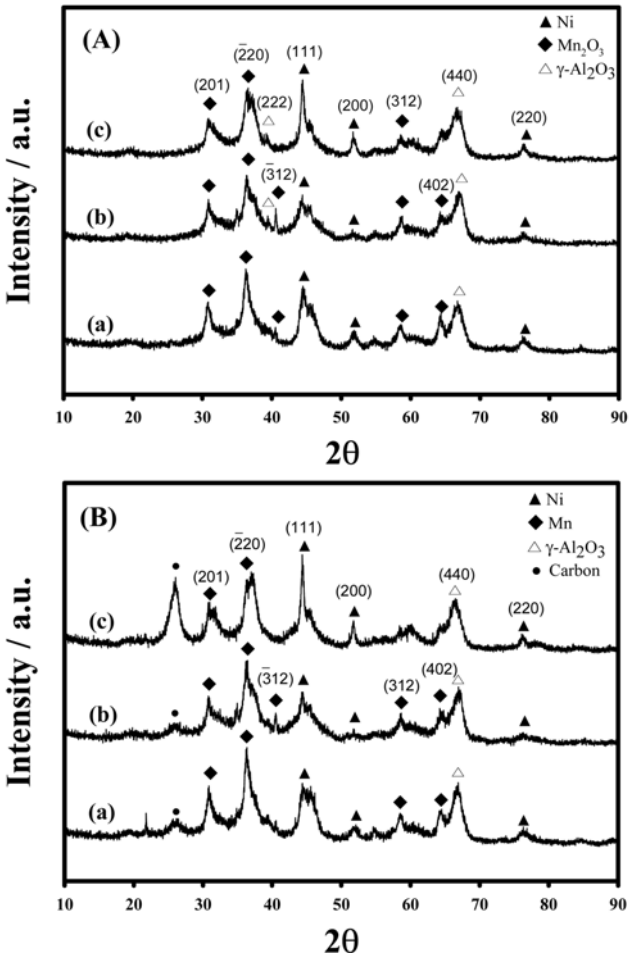

Fig. 6. X-ray diffraction patterns for the Mn-promoted Ni/γ-Al_2O_3 catalysts, viz. 5.3 wt% Mn/5.4 wt% Ni/γ-Al_2O_3 (a), 4.0 wt% Ni/4.5 wt% Mn/γ-Al_2O_3 (b), and 4.2 wt% Mn-4.2 wt% Ni/γ-Al_2O_3 (c) before (A) and after the reaction (B).

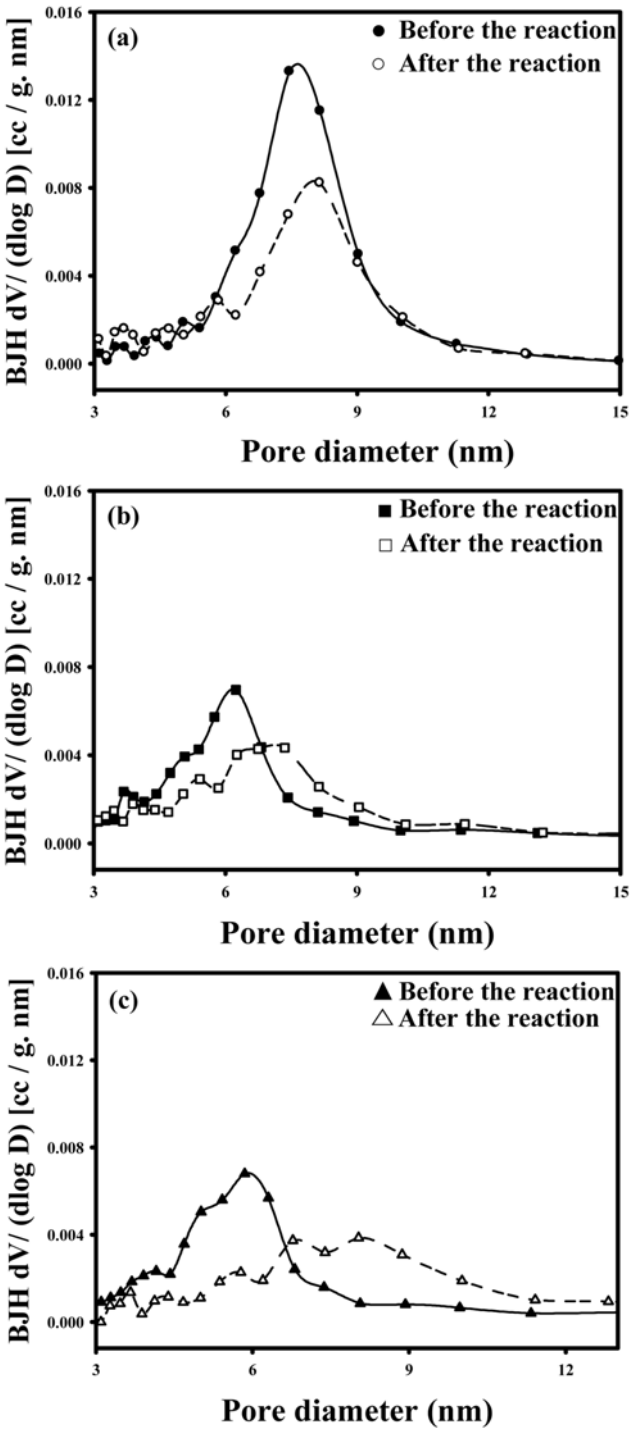

Fig. 7. Pore size distribution of the Mn-promoted Ni/γ-Al_2O_3 catalysts, viz. 5.3 wt% Mn/5.4 wt% Ni/γ-Al_2O_3 (a), 4.0 wt% Ni/4.5 wt% Mn/γ-Al_2O_3 (b), and 4.2 wt% Mn-4.2 wt% Ni/γ-Al_2O_3 (c) before (closed symbol) and after the reaction at 873 K for 10 h (open symbol).

be to remove the large ensembles of Ni atoms active for the coke formation process. From this viewpoint, it is reasonable to suppose that the least coke formation occurs over Mn/Ni/γ-Al_2O_3 because the largest portion of MnO_x species can reside on Ni over this catalyst among the Mn-promoted Ni/γ-Al_2O_3 catalysts.

The pore size distribution was obtained from the N_2 desorption data for the Mn-promoted Ni/γ-Al_2O_3 catalysts before and after the reaction, as shown in Fig. 7. No noticeable difference in the pore size distribution was observed over 5.3 wt% Mn/5.4 wt% Ni/γ-Al_2O_3 during the reaction. On the other hand, the average pore sizes increased for 4.2 wt% Mn-4.2 wt% Ni/γ-Al_2O_3 and 4.0 wt% Ni/4.5 wt% Mn/γ-Al_2O_3 during the reaction. It can be said that the small pores are blocked and larger pores are newly formed during the reaction for these catalysts. As revealed by the CHNS analysis, a large amount of carbon was accumulated over these catalysts during the reaction, and thus can cause pore blocking.

To detect any change in the surface composition during the reaction, the XPS spectra were obtained for the Mn-promoted Ni/γ-Al_2O_3 catalysts before and after the reaction, as shown in Fig. 8. Various oxidation states of Mn such as Mn^{4+}, Mn^{3+} and Mn^{2+} can be assigned for all of the catalysts based on the Mn2p spectra. 5.3 wt% Mn/5.4 wt% Ni/γ-Al_2O_3 shows the highest proportion of Mn^{4+} species compared with the other Mn-promoted Ni/γ-Al_2O_3 catalysts. For all of the catalysts, the proportion of Mn^{2+} and Mn^{3+} increases compared to that of Mn^{4+} during the reaction. This tendency was obvious especially for 4.2 wt% Mn-4.2 wt% Ni/γ-Al_2O_3 and 4.0 wt% Ni/4.5 wt%

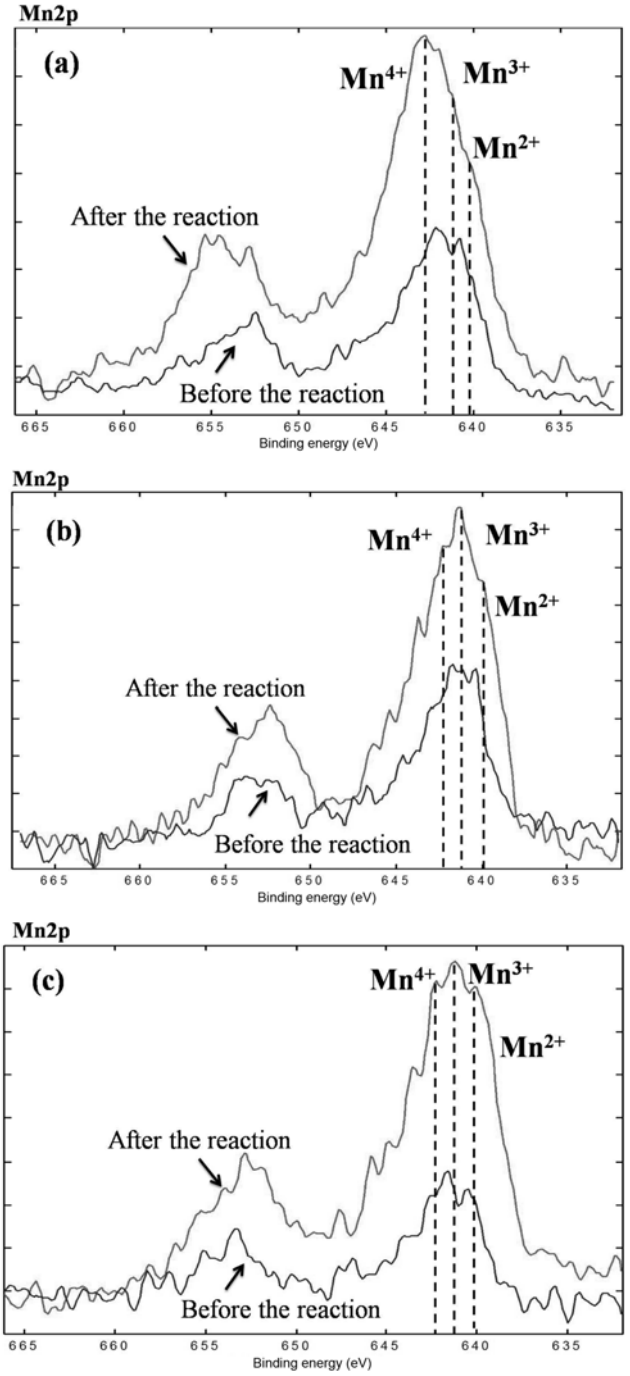

Fig. 8. XPS spectra of the Mn-promoted Ni/γ-Al_2O_3 catalysts, viz. 5.3 wt% Mn/5.4 wt% Ni/γ-Al_2O_3 (a), 4.0 wt% Ni/4.5 wt% Mn/γ-Al_2O_3 (b), and 4.2 wt% Mn-4.2 wt% Ni/γ-Al_2O_3 (c) before and after the reaction at 873 K for 10 h.

Mn/γ-Al_2O_3. Based on these results, the stable catalytic activity of 5.3 wt% Mn/5.4 wt% Ni/γ-Al_2O_3 may be partly ascribed to the higher oxidation states of the manganese oxides.

CONCLUSIONS

4.1 wt% Ni/γ-Al_2O_3 showed stable catalytic activity with the least amount of coke formation among the Ni/γ-Al_2O_3 catalysts containing 3.1 wt%, 4.1 wt% and 8.1 wt% Ni. The addition of manganese oxides to Ni/γ-Al_2O_3 changed its catalytic activity and stability, which were strongly dependent on the impregnation sequence of the Ni and Mn precursors. Among the Mn-promoted Ni/γ-Al_2O_3 catalysts, 5.3 wt% Mn/5.4 wt% Ni/γ-Al_2O_3 showed stable catalytic activity with the least amount of coke formation. It also exhibited a similar H_2 formation rate to the 4.1 wt% Ni/γ-Al_2O_3 catalyst. The catalytic activity increased with increasing amount of chemisorbed CO for the Mn-promoted Ni/γ-Al_2O_3 catalysts. The highest proportion of Mn^{4+} species was observed for the most stable catalyst.

ACKNOWLEDGEMENT

This work was supported by the Priority Research Centers Program through the National Research Foundation of Korea (NRF) funded by the Ministry of Education, Science and Technology (2009-0094047).

REFERENCES

1. C. Song, *Catal. Today*, **77**, 17 (2002).
2. G. Kolb, R. Zapf, V. Hessel and H. Lowe, *Appl. Catal. A: Gen.*, **277**, 155 (2004).
3. K. Ahmed, J. Gamman and K. Föger, *Solid State Ion*., **152**, 485 (2002).
4. J. D. Holladay, E. O. Jones, M. Phelps and J. Hu, *J. Power Sources*, **108**, 21 (2002).
5. R. Craciun, B. Sheeck and R. J. Gorte, *Catal. Lett*., **51**, 149 (1998).
6. Q. Ming, T. Healey, L. Allen and P. Lrving, *Catal. Today*, **77**, 51 (2002).
7. K. Geissler, E. Newson, F. Vogel, T. B Truong and P. Hottinger, *Phys. Chem. Chem. Phys.*, **3**, 289 (2001).
8. S. Ayabe, H. Omoto and T. Utaka, *Appl. Catal. A: Gen*., **241**, 261 (2003).
9. P. K. Cheekatamarla and C. M. Finnerty, *J. Power Sources*, **160**, 490 (2006).
10. J. R. Rostrup-Nielsen, *Catal. Today*, **18**, 305 (1993).
11. S. Natesakhaway, R. B. Watson and X. Wang, *J. Catal*., **234**, 496 (2005).
12. J. T. Richardson and J. L. Propp, *J. Catal*., **98**, 457 (1986).
13. P. Wynblatt and N. A. Gjoestein, *Prog. Solid State Chem*., **9**, 21 (1975).
14. Z. Zhang and X. E. Verykios, *Appl. Catal. A: Gen*., **138**, 109 (1996).
15. J. M. Wei, B. Q. Xu, J. L. Li, Z. X. Cheng and Q. M. Zhu, *Appl. Cata. A: Gen*., **196**, L167 (2000).
16. L. B. Råberg, M. B. Jensen, U. Olsbye, C. Daniel and S. Haag, *J. Catal*., **249**, 250 (2007).
17. D. L. Trimm, *Catal. Today*, **37**, 233 (1997).
18. S. Wang and G. O. M. Lu, *Appl. Catal. B: Environ*., **16**, 269 (1998).
19. T. Horiuchi, K. Sakuma, T. Fukui, T. Osaki and T. Mori, *Appl. Catal. A: Gen*., **144**, 111 (1996).
20. M. C. J. Bradford and M. Vannice, *Appl. Catal. A: Gen*., **142**, 73 (1996).
21. Y. H. Hu, O. Yamazaki, K. Tomishige and K. Fujimoto, *Catal. Lett*., **39**, 91 (1996).
22. Y.-G. Chen, K. Tomishige, K. Yokoyama and K. Fujimoto, *J. Catal*., **184**, 479 (1999).

23. K. Tomishige, Y.-G. Chen and K. Fujimoto, *J. Catal*., **181**, 91 (1999).
24. K. O. Christensen, D. Chen, R. Lødeng and A. Holmen, *Appl. Catal. A: Gen*., **314**, 9 (2006).
25. Z. Hou, O. Yokota, T. Tanaka and T. Yashima, *Appl. Catal. A: Gen*., **253**, 381 (2003).
26. B. L. Su, S. D. Guo, in Delmen, G. F. Formment (Eds.), Catalyst Deactivation, Elsevier, Amsterdam, 325 (1999).
27. D. L. Trimm, *Catal. Today*, **49**, 3 (1999).
28. S. Natesukhanat, R. B. Watson and X. Wang, *J. Catal*., **234**, 496 (2005).
29. S. Natesakhawat, O. Oktar and U. S. Ozkan, *J. Mol. Catal. A-Chem*., **241**, 133 (2005).
30. S. H. Seok, S. H. Choi, E. D. Park and J. S. Lee, *J. Catal*., **209**, 6 (2002).
31. L. Chmielarz, P. Kustrowski and R. Dziembaj, *Thermochm. Acta*, **395**, 225 (2002).
32. K. Schulze, W. Makowski and R. Chyzi, *Appl Clay. Sci.*, **18**, 59 (2001).
33. J.-H. Kim, D. J. Suh, T.-J. Park and K.-L. Kim, *Appl. Catal. A: Gen*., **197**, 191 (2000).